JOURNAL OF VIROLOGY, July 2009, p. 6404–6415 Vol. 83, No. 13
0022-538X/09/$08.00+0 doi:10.1128/JVI.00126-09

Development and Characterization of a Mouse Model for Marburg Hemorrhagic Fever▽

Kelly L. Warfield,* Steven B. Bradfute, Jay Wells, Loreen Lofts, Meagan T. Cooper, D. Anthony Alves, Daniel K. Reed, Sean A. VanTongeren, Christine A. Mech, and Sina Bavari*

United States Army Medical Research Institute of Infectious Diseases, Fort Detrick, Maryland 21702

Received 19 January 2009/Accepted 1 April 2009

The lack of a mouse model has hampered an understanding of the pathogenesis and immunity of Marburg hemorrhagic fever (MHF), the disease caused by marburgvirus (MARV), and has created a bottleneck in the development of antiviral therapeutics. Primary isolates of the filoviruses, i.e., ebolavirus (EBOV) and MARV, are not lethal to immunocompetent adult mice. Previously, pathological, virologic, and immunologic evaluation of a mouse-adapted EBOV, developed by sequential passages in suckling mice, identified many similarities between this model and EBOV infections in nonhuman primates. We recently demonstrated that serially passaging virus recovered from the liver homogenates of MARV-infected immunodeficient (SCID) mice was highly successful in reducing the time to death in these mice from 50 to 70 days to 7 to 10 days after challenge with the isolate MARV-Ci67, -Musoke, or -Ravn. In this study, we extended our findings to show that further sequential passages of MARV-Ravn in immunocompetent mice caused the MARV to kill BALB/c mice. Serial sampling studies to characterize the pathology of mouse-adapted MARV-Ravn revealed that this model is similar to the guinea pig and nonhuman primate MHF models. Infection of BALB/c mice with mouse-adapted MARV-Ravn caused uncontrolled viremia and high viral titers in the liver, spleen, lymph node, and other organs; profound lymphopenia; destruction of lymphocytes within the spleen and lymph nodes; and marked liver damage and thrombocytopenia. Sequencing the mouse-adapted MARV-Ravn strain revealed differences in 16 predicted amino acids from the progenitor virus, although the exact changes required for adaptation are unclear at this time. This mouse-adapted MARV strain can now be used to develop and evaluate novel vaccines and therapeutics and may also help to provide a better understanding of the virulence factors associated with MARV.

The filoviruses, *Marburgvirus* and *Ebolavirus* (MARV and EBOV), cause severe hemorrhagic fevers in humans and nonhuman primates (27). The incubation time is estimated to be 3 to 21 days, with human case fatality rates reaching 90% in some outbreaks. Filoviral hemorrhagic fevers are characterized by a nonspecific viral prodrome in the early stage of infection, including fever, headaches, and myalgia (27). This is followed by a hemorrhagic phase that can include development of a maculopapular rash, petechiae, and bleeding from the gums, intestines, and other mucosal surfaces. Death usually occurs within a week of initial symptoms and is thought to be due to uncontrolled viral replication, hypotension-induced shock caused by increased vascular permeability, and multiorgan failure, likely caused by disseminated intravascular coagulation and extensive necroses in the liver, spleen, intestine, and many other major organ systems (27).

Human-derived MARVs (isolates Angola, Musoke, Ravn, and Ci67) do not kill immunocompetent adult mice (23). Furthermore, there are no published reports of any lethal mouse-adapted MARV. The current mouse-adapted EBOV, strain Zaire (ZEBOV), was developed by performing nine sequential passages of ZEBOV 1976 virus in suckling mice, followed by two sequential plaque picks. The resulting virus was uniformly lethal to mice inoculated intraperitoneally (i.p.). Pathological evaluation of infected mice identified many similarities and only a few differences between this model (7, 22) and infections in nonhuman primates (21).

In a previous study, we took a slightly different approach to mouse adaptation of MARV and found that serially passaging virus recovered from the liver homogenates of MARV-Ravn-infected adult mice with severe combined immunodeficiency (SCID mice) resulted in the generation of SCID-adapted MARV-Ravn (scid-MARV) that rapidly killed SCID mice but did not kill adult immunocompetent mice (51). In this study, we used scid-MARV as starting material for the first round of infection of adult immunocompetent BALB/c mice and serially passaged virus recovered from the liver homogenates of the BALB/c mice. MARV-Ravn was chosen over SCID-adapted MARV-Ci67 or -Musoke because it adapted more rapidly to SCID mice than the other isolates did. This produced a mouse-adapted MARV-Ravn strain (ma-MARV) that could kill adult BALB/c mice. Serial sampling studies to characterize the pathogenesis of ma-MARV revealed that this model was very similar to the guinea pig and nonhuman primate Marburg hemorrhagic fever (MHF) models, including rapid viremia,

* Corresponding author. Present address for Kelly L. Warfield: Integrated BioTherapeutics Inc., 20358 Seneca Meadows Parkway, Germantown, MD 20876. Phone: (240) 454-8936. Fax: (240) 515-0324. E-mail: kelly@integratedbiotherapeutics.com. Mailing address for Sina Bavari: USAMRIID, 1425 Porter Street, Fort Detrick, MD 21702. Phone: (301) 619-4246. Fax: (301) 619-2290. E-mail: sina.bavari@us.army.mil.

▽ Published ahead of print on 15 April 2009.

induction of D-dimers (fibrin degradation products), thrombocytopenia, profound loss of circulating and tissue lymphocytes, and marked liver damage. Additionally, we compared the immunological responses of mice after infection with either nonadapted wild-type MARV-Ravn (wt-MARV) or ma-MARV. This mouse model of MARV infection not only should advance our understanding of MARV pathogenesis and immunity but also may play a critical role in discovery of therapeutics for MARV infection.

MATERIALS AND METHODS

Virus and cells. Primary human-derived wt-MARV and ma-MARV-Ravn were propagated in Vero or VeroE6 cells, and plaques were counted by a standard plaque assay on Vero cells (33). MARV-infected cells and animals were handled in a biosafety level 4 (BSL-4) laboratory at the United States Army Medical Research Institute of Infectious Diseases.

Animals. BALB/c mice aged 6 to 10 weeks, of either gender, were obtained from the National Cancer Institute, Frederick Cancer Research and Development Center (Frederick, MD). Mice were housed in microisolator cages and provided autoclaved water and chow ad libitum. Research was conducted in compliance with the Animal Welfare Act and other federal statutes and regulations relating to animals and experiments involving animals and adhered to principles stated in the *Guide for the Care and Use of Laboratory Animals* (34a). The facility where this research was conducted is fully accredited by the Association for Assessment and Accreditation of Laboratory Animal Care International.

Mouse adaptation. The general approach to adapt MARV to lethality in mice was to start with the virus previously adapted to SCID mice, which had an increased virulence compared to that of the progenitor wt-MARV (51), and then to passage the virus in BALB/c mice to develop a lethal mouse-adapted MARV. The goal was to isolate a virus capable of migrating and replicating in the liver at the earliest time point. To start, the SCID-adapted MARV-Ravn strain, which had been passaged 10 times in SCID mice (51), was injected i.p. into 10 6- to 10-week-old immunocompetent BALB/c mice. On day 3 or 4, two mice were euthanized, and the livers were removed, pooled, and homogenized in 10 ml of phosphate-buffered saline. Upon each passage, the liver homogenates were injected i.p. ("passaged") (200 μl) into naïve mice. Lethal viruses were then isolated by plaque purification from the livers of the BALB/c mice that succumbed to infection (after 24 total passages in SCID and BALB/c mice). None of the liver homogenates before passage 24 killed BALB/c mice.

Viral RNA extraction, cDNA synthesis, and nucleic acid sequence determination. Viral RNA was extracted from Trizol LS reagent (Invitrogen Corp.)-treated viral stocks. The final ma-MARV-Ravn strain was plaque purified three times before seed stock production. Liver homogenates from the last three BALB/c passages were also treated with Trizol LS reagent; however, these were not plaque purified before RNA extraction. cDNA was synthesized from viral RNA by reverse transcription-PCR by using standard methods and random primers.

Nucleotide sequences were determined by primer walking the entire genome by use of oligonucleotide primers designed from the MARV-Ravn guinea pig lethal variant published sequence (GenBank accession no. EF446131), using Lasergene Primer Select v:7.2.1(1), 410 (DNASTAR, Inc.). The termini of all genomes were sequenced with the gene-specific primer extrapolated from the published sequence that was used to generate the amplimer. The remaining genomic nucleotide sequences were determined from overlapping PCR amplimer contigs, using an ABI Prism BigDye Terminator cycle sequencing ready reaction kit (v1.0 or v3.1; Applied Biosystems) per the manufacturer's instructions for amplimers. Nucleic acid sequence determination was performed with an ABI Prism 3730 DNA analyzer, and the resultant contigs were assembled with Lasergene SeqMan II, v:7.2.1(1), 410 software for Microsoft Windows (DNASTAR, Inc.). Transcribed and translated nucleic acid and deduced amino acid sequences were aligned and percent identities calculated using LaserGene MegAlign Clustal W v:7.2.1(1), 410 (DNASTAR, Inc.).

Viral challenges with mouse-adapted MARV. For characterization studies, BALB/c mice (unless otherwise indicated) were injected i.p. with ~1,000 PFU of wt or mouse-adapted MARV-Ravn. To determine the lethality of the mouse-adapted MARV-Ravn strain, mice were inoculated with 1,000 or 100,000 PFU by i.p., subcutaneous (at the base of the neck or tail), intramuscular, footpad, or intranasal inoculation. All inoculations were done in a volume of 100 μl, except for footpad inoculation, which was carried out with 20 μl. After challenge, mice were observed at least twice daily for illness and death, and in some experiments, daily weights were determined for each infected group. Mice considered moribund were euthanized based on set criteria (weight loss, reduced grooming, anorexia, and decreased activity and responsiveness).

Serial sampling studies. Five animals were randomly chosen to be euthanized at 0 to 7 days postchallenge for necropsy. Blood samples were obtained under anesthesia by cardiac puncture. Viremia or tissue viral titers were determined by traditional plaque assay (33). Hematological, cytokine (mouse 25-plex cytokine kit; Biosource/Invitrogen), alpha interferon (IFN-α) (Biosource/Invitrogen), and D-dimer levels (Diagnostica Stago), as well as liver-associated enzyme levels, were measured as previously described (19, 52). Clotting times (prothrombin time [PT] and activated partial thromboplastin time [aPTT]) were determined using ThromboScreen (Fisher Diagnostics). Tissues from each mouse were collected in 10% neutral buffered formalin and held in the BSL-4 laboratory for >21 days. The tissues were embedded in paraffin, sectioned for histology, and stained with hematoxylin and eosin for routine light microscopy or stained with MARV-specific antisera to identify viral antigen.

Flow cytometry. Cardiac puncture was used to acquire blood from anesthetized mice into EDTA tubes. For lymphocyte number and other hematologic analyses, blood was analyzed with an ACT 10 counter (Coulter, Fullerton, CA). Remaining blood or a single-cell suspension of mouse splenocytes was lysed with red blood cell lysing buffer (Sigma, St. Louis, MO) and washed with RPMI medium containing 2% fetal calf serum. For both blood cells and splenocytes, antibodies (purchased from eBioscience, San Diego, CA, and BD Biosciences, San Jose, CA) were added at 1:100, incubated for 15 min at 4°C, and then washed. Cells were analyzed in BSL-4 containment with a FACSCanto II flow cytometer (BD Biosciences, San Jose, CA).

Statistical analysis. Paired Student's *t* test was used to directly compare samples from MARV-infected and mock-infected mice. *P* values of ≤0.05 were considered significant.

Nucleotide sequence accession numbers. MARV-Ravn sequences were submitted to GenBank on 19 February 2008 and were given the following accession numbers: MARV-Ravn progenitor, EU500827; and mouse-adapted MARV-Ravn, EU500826.

RESULTS

Adaptation of MARV to BALB/c mice. Twenty-four sequential passages of MARV-Ravn (10 passages in SCID mice and then 14 passages in BALB/c mice) generated a MARV-Ravn strain that was lethal to adult immunocompetent BALB/c mice (ma-MARV). No lethality or morbidity was observed in BALB/c mice by any of the MARV isolates in passages before passage 24. To verify the lethality of the plaque-purified ma-MARV, BALB/c mice were injected i.p. with ~1,000 PFU of ma-MARV (Fig. 1A). To determine which routes of infection were lethal, BALB/c mice were infected via different routes with ma-MARV. Interestingly, the mice that were infected via the i.p. or intranasal route lost a significant amount of weight, while those injected subcutaneously (base of neck or tail), in the footpad, or intramuscularly did not (Fig. 1B). Only i.p. injection of BALB/c mice caused lethal disease among the many routes tested, and this was true with both 1,000- and 100,000-PFU challenge doses (data not shown). i.p. injected mice became ruffled, hunched, and lethargic prior to succumbing to infection; bleeding was not observed. Similarly, mouse-adapted EBOV causes lethality only when it is injected via the i.p. route (7). Differences in lethality for various infection routes may be due to rapid uptake of the virus by phagocytic cells in the peritoneal cavity, lack of induction of innate immunity following i.p. administration, differential control of the virus by peripheral lymph nodes, and differences in virus distribution (systemic versus localized) following different inoculation routes (7).

Growth of wt-MARV and ma-MARV in mice. To determine the virologic, pathological, and immunologic differences in wt-MARV and ma-MARV, serial sampling studies were carried

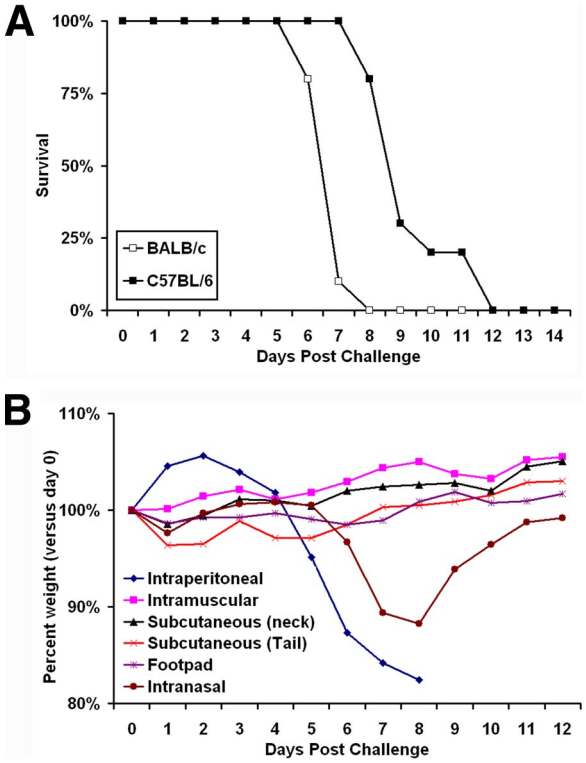

FIG. 1. Survival of mice inoculated with mouse-adapted MARV-Ravn. (A) BALB/c mice ($n = 10$) were injected i.p. with ~1,000 PFU of mouse-adapted MARV-Ravn diluted in phosphate-buffered saline. The survival data for each group are presented on a Kaplan-Meier curve. (B) Weight loss data after BALB/c mice were challenged via i.p., intranasal, subcutaneous (base of neck or tail), footpad, and intramuscular routes with 1,000 PFU. The weights of groups of 10 mice were assessed daily after infection with the mouse-adapted MARV-Ravn strain. The data are expressed as the average weight of the mice in each group. Only the mice infected i.p. succumbed to infection.

out. Viral replication in sera or tissue homogenates from infected BALB/c mice was assessed using a standard plaque assay. Viremia was detected sooner in ma-MARV-infected mice, as early as day 1, than in mice infected with wt-MARV (Fig. 2A). Additionally, the viral titers in the blood peaked at much higher levels for the lethal ma-MARV-infected mice than for wt-MARV-infected mice (Fig. 2A); this was also true for all other tissues assayed, with the exception of the spleen, where the peak viral titers for mouse-adapted and wt viruses were similar (Fig. 2B to I). The other notable difference in viral titers between the ma- and wt-MARV-Ravn-infected mice was the rate of viral clearance, as the wt-MARV-infected mice appeared to resolve the viral infection around day 6. In the liver, spleen, kidneys, lungs, and gonads, the virus was readily detectable by day 3 after infection with ma-MARV and increased steadily until the time of death. In the mesenteric lymph nodes, brain, and intestine, virus was not detectable until later times in the ma-MARV-infected mice.

Pathology. Compared to the spleens of uninfected mice (Fig. 3A), there was diffuse but mild lymphoid depletion in both the periarteriolar lymphoid sheaths (PALS) and follicles in ma-MARV-infected mice, without histologic evidence of lymphocytolysis, at 2 and 3 days postinfection (Fig. 3B). There was also congestion of the red pulp and loss of the compartment where mice normally have extramedullary hematopoiesis. This also included a loss of megakaryocytes, the source of new platelets. By day 4, moderate lymphoid depletion with increased numbers of apoptotic-like bodies and tingible body macrophages, consistent with lymphocytolysis, was observed in the PALS and follicles (Fig. 3C and D). The splenic lymphoid depletion and, particularly, lymphocytolysis progressively worsened in mice through day 7, with increased numbers of apoptotic-like bodies and tingible body macrophages being observed in the splenic red pulp (data not shown). Large lymphoblastic cells were also noted in the splenic marginal zones on days 5, 6, and 7. In contrast to the case for uninfected mice (Fig. 3E), rounded-up hepatocytes with hypereosinophilic cytoplasm and pyknotic nuclei, interpreted as single-cell hepatocellular necrosis, were randomly scattered throughout the hepatic parenchyma of ma-MARV-infected mice at day 3 postinfection (Fig. 3F). On days 4, 5, and 6, hepatic lesions consistently and progressively worsened, characterized by extensive lipid-type vacuolar changes (fatty degeneration) and single-cell hepatocellular necrosis, with occasional pleomorphic eosinophilic intracytoplasmic inclusion bodies and multifocal to coalescing areas of neutrophilic inflammation mixed with cellular debris (Fig. 3G and H). By day 7, few normal hepatocytes were observed histologically (data not shown). In contrast, drastic pathological changes, including severe lymphocytolysis and lymphoid depletion in the spleen and hepatocellular degeneration and necrosis in the spleen and liver, were not observed in wt filovirus-infected mice.

By immunohistochemistry, and in contrast to the case for uninfected mice (Fig. 4A), rare ma-MARV-infected splenic cells were observed on day 1 (data not shown), with a slight increase in immunopositive cells by day 2 (Fig. 4B). The strongest and most significant splenic immunostaining was observed on day 3, in the marginal zones near the B-cell follicles and within the perilymphoid (perifollicular) red pulp of infected mice, localized to cells morphologically suggestive of macrophages and/or dendritic cells (Fig. 4C). There was decreased viral antigen staining on days 4 and 5 (Fig. 4D), and almost no antigen was observed in any ma-MARV-infected mice by days 6 and 7, except on the splenic capsule (Fig. 3E and F). In contrast to the case for uninfected mice (Fig. 4G), rare ma-MARV-infected liver cells were observed on day 1 (data not shown), with a slight increase in MARV-positive cells by day 2 or 3 (Fig. 4H and data not shown). The strongest and most significant liver immunostaining was observed on days 4 to 6 (Fig. 4J to L and data not shown). Similar to observations in the spleen, there was decreased viral antigen staining at day 7 in the liver (data not shown).

Clinical laboratory changes in ma-MARV-infected mice. Hematologic analysis revealed a decrease in peripheral white blood cell counts in mice infected with ma-MARV on days 3 to 5 after infection (Fig. 5A). Similarly, peripheral lymphocyte numbers fell in ma-MARV-infected mice on days 3 and 5 postinfection and recovered on day 7 (Fig. 5B and C). This drop and subsequent recovery in peripheral lymphocyte numbers have been reported for EBOV-infected primates and mice (5, 21, 38). Mice infected with wt-MARV did not have a statistically significant difference in peripheral white blood cell or lymphocyte number over the course of infection. Liver and

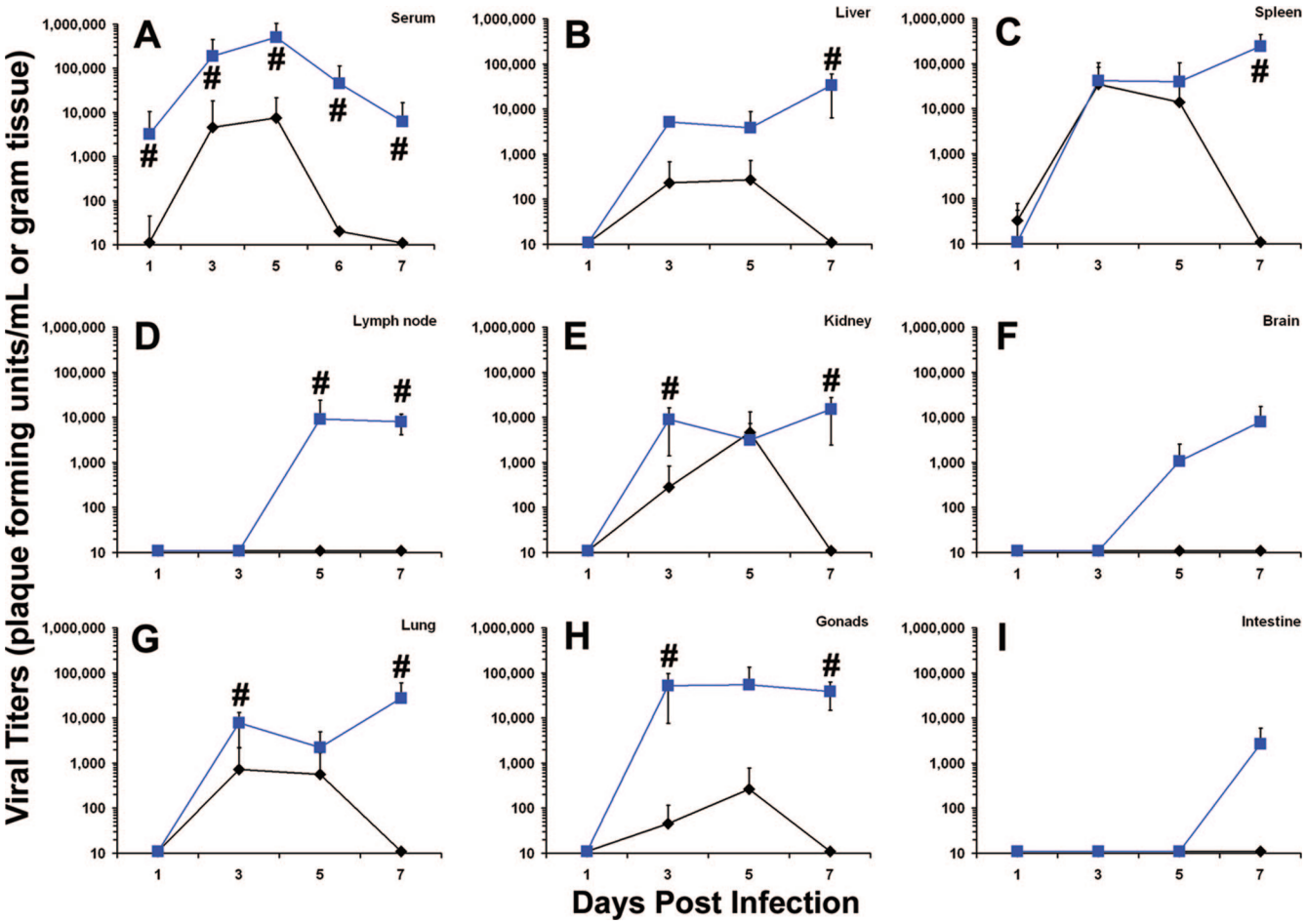

FIG. 2. Replication of wt or mouse-adapted MARV in mice. Mice were infected with 1,000 PFU of wt or mouse-adapted MARV-Ravn, and sera were collected at the indicated times. Viral titers were measured using a standard plaque assay on serum samples obtained from terminal cardiac punctures (A) or 10% tissues homogenates of liver (B), spleen (C), lymph node (D), kidney (E), brain (F), lung (G), gonads (H), and intestine (I). Data are expressed as the average of values for four or five mice/time point, and error bars indicate standard deviations. Black lines, wt-MARV-Ravn-infected mice; blue lines, mouse-adapted MARV-Ravn-infected mice. #, $P \leq 0.05$ (comparing wt and mouse-adapted MARV-Ravn strains).

kidney functions were analyzed by measuring levels of alanine transaminase (ALT), aspartate transaminase (AST), amylase, alkaline phosphatase (ALP), blood urea nitrogen (BUN), and glucose in serum. As shown in Fig. 5D to I, liver and kidney functions were both greatly diminished, as revealed by increased ALT, AST, ALP, and BUN levels and decreased glucose levels in ma-MARV-infected mice, whereas mice infected with wt-MARV-Ravn were not affected.

Platelet levels in ma-MARV-infected mice decreased drastically starting at day 5 postinfection, while wt-MARV-infected animals showed no significant difference in platelet counts compared to uninfected mice (Fig. 6A). Consistent with alterations in coagulopathy, we also noted elevated D-dimer levels in ma-MARV-infected mice but not in wt-MARV-infected animals (Fig. 6B). However, we did not note significant fibrin deposition in tissues by electron microscopy (data not shown). Furthermore, no change in PT with either mouse-adapted MARV or wt-MARV infection was noted compared to naïve mice (day 0). However, by day 5, we noted a drop in the aPTT for mouse-adapted MARV- but not wt-MARV-infected mice compared to uninfected mice. This is a curious observation given the concurrent rise in D-dimer levels and drop in platelet levels, and it warrants further investigation.

Immunologic responses to wt-MARV or mouse-adapted MARV. Total numbers of white blood cell subsets in blood (Fig. 7) were determined by flow cytometry for infected animals and compared to the numbers for uninfected animals. Peripheral numbers of $CD4^+$, $CD8^+$, B, and NK cells in ma-MARV-infected mice were decreased relative to those in wt-MARV-infected mice (Fig. 7A to D). Peripheral macrophages and dendritic cell numbers in the blood and spleen increased on day 7 in ma-MARV-infected mice (Fig. 7E and F and data not shown). In the spleens of infected mice, there was a drop in the percentage of NK cells ($DX5^+$ $CD3^-$) and $CD4^+$ $CD44^{hi}$ cells (activated $CD4^+$ cells) in mouse-adapted MARV- but not wt-MARV-infected BALB/c mice (data not shown). We also observed increases in NK and $CD8^+$ cells that were $CD44^{hi}$ in mouse-adapted MARV-infected mice and lesser increases in wt-MARV-infected mice. These cellular changes

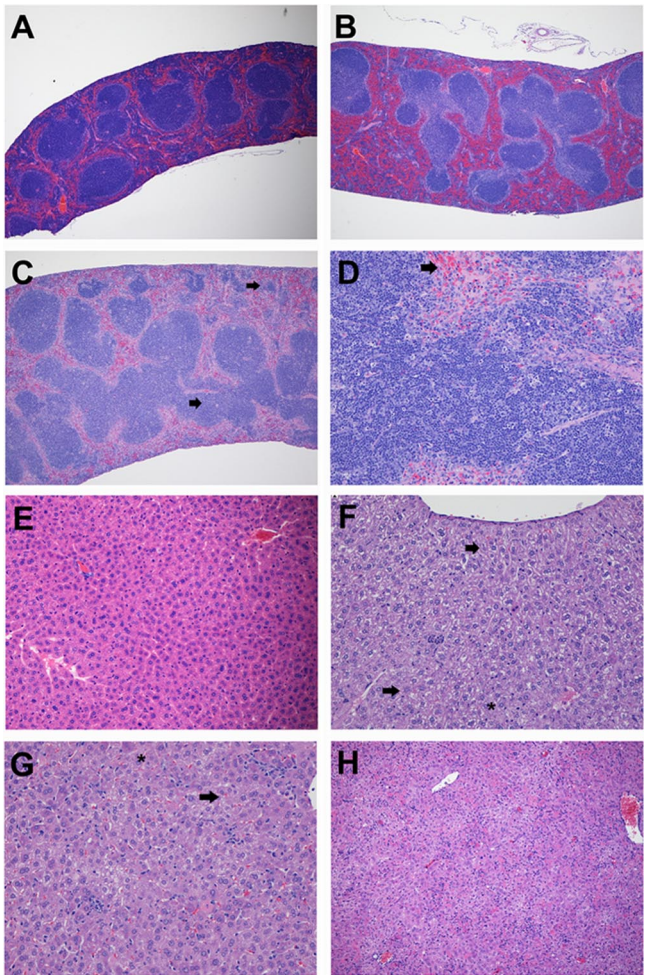

FIG. 3. Histological changes in spleens and livers of mice infected with MARV. BALB/c mice were challenged i.p. with 1,000 PFU of mouse-adapted MARV-Ravn, and tissue samples were collected on days 0, 1, 2, 3, 4, 5, 6, and 7 after challenge ($n = 4$/group). The spleens from the MARV-infected mice were stained with hematoxylin and eosin, and representative pictures from days 0 (A), 2 (B), and 4 (C and D) are shown. The livers from the MARV-infected mice were also stained with hematoxylin and eosin, and representative pictures from days 0 (E), 3 (F), 5 (G), and 6 (H) are shown. (A) The control (uninfected) mouse sampled at day 0 showed normal splenic morphology. (B) On day 2, noticeable white pulp pallor (PALS and follicles) suggestive of mild lymphoid depletion was observed in the spleens from MARV-infected mice. There was also diffuse red pulp congestion. (C and D) The lymphoid depletion continued to worsen, and by day 4, the first histologic evidence of necrotic/apoptotic lymphocytes and tingible body macrophages was observed. In comparison to day 2, on day 4 there was decreased red pulp cellularity, with an increased amount of necrotic/apoptotic debris (arrowheads). (E) The control (uninfected) mouse sampled at day 0 showed normal hepatic morphology. (F) On day 3, individual necrotic hepatocytes (arrowheads) were occasionally observed scattered throughout the hepatic parenchyma. By day 4, and extending through days 5 (G), 6 (H), and 7 (not shown), histologic lesions consistently present in livers from MARV-infected mice included moderate to severe vacuolar changes (fatty degeneration [asterisk]), single-cell hepatocellular necrosis (arrowhead), eosinophilic intracytoplasmic inclusion bodies, and multifocal to coalescing areas of neutrophilic inflammation admixed with cellular debris. Magnification, ×4 for panels A to C, ×10 for panel H, and ×20 for panels D to G.

were similar to those observed in mouse-adapted EBOV infection (5).

As part of our characterization, we broadly assayed cytokine responses to wt and mouse-adapted MARV-Ravn infection (Fig. 8). Most of the cytokines were not modulated in the sera of BALB/c mice after wt-MARV infection. For ma-MARV-infected mice, increases in almost every inflammatory (MCP-1, MIG, IP-10, KC, MIP-1 alpha, and interleukin-6 [IL-6]), Th1 (IFN-γ and IL-12), and Th2 (IL-5, IL-10, and IL-13) cytokine assayed were observed relative to those in wt-MARV-infected mice (Fig. 8). Interestingly, transient increases in IFN-α were observed in the ma-MARV-Ravn-infected mice compared to wt-MARV-Ravn-infected mice (Fig. 8). These data suggest an ineffective immune response to lethal ma-MARV-Ravn infection but not to infection with wt-MARV. It is important that cytokine levels measured in serum are only crude indicators of local antiviral immune responses.

Mutations identified in mouse-adapted virus variants. In order to identify the mutations in mouse-adapted MARV-Ravn, the genomic nucleotide sequences were compared to those of a human isolate which is nonlethal in mice but 100% lethal in macaques (11). There were 61 nucleotide differences identified in ma-MARV compared with the wt-MARV isolate. The nucleotide differences in viral variants are listed in Table 1. A majority of the nucleotide differences were thymine-to-cytosine changes (90% for ma-MARV), which in addition to the other transversions and transitions were all located in the nucleoprotein, VP35, VP40, and VP30 coding regions and the VP35-VP40 and GP-VP30 intergenic regions. There were no nucleotide changes in leader/trailer, glycoprotein (GP), and RNA-dependent RNA polymerase (L) coding regions or in other intergenic regions. The percentage of the nucleotide differences predicted to cause amino acid mutations was 23% for the ma-MARV variant. The predicted amino acid differences among the wt and mouse-adapted viral variants are listed in Table 1.

DISCUSSION

This is the first report of a lethal immunocompetent mouse model for study of vaccines, therapeutics, pathogenesis, and immunity for MHF. The development of a MARV-Ravn lethal infection model with adult BALB/c mice was achieved by serially passaging virus recovered from the livers of MARV-infected mice until lethality was achieved after a total of 24 mouse passages. Pathogenesis studies of the mouse-adapted MARV strain in BALB/c mice revealed that this novel mouse-adapted MARV model has many similarities to guinea pig and nonhuman primate MHF models, including uncontrolled viral growth in every tissue assayed, changes in coagulation function, profound destruction of circulating and tissue lymphocytes, and marked liver damage.

Based on EBOV adaptation data for mice, we would have predicted changes in VP24, NP, and L to be important (12, 50). However, we found a combination of changes in VP40 ($n = 7$ amino acid differences), VP35 ($n = 5$ amino acid differences), NP, and VP30 ($n = 1$ amino acid difference in each protein) in ma-MARV-Ravn compared to the primary isolate from which it was derived (Table 1). The relationship of the identified

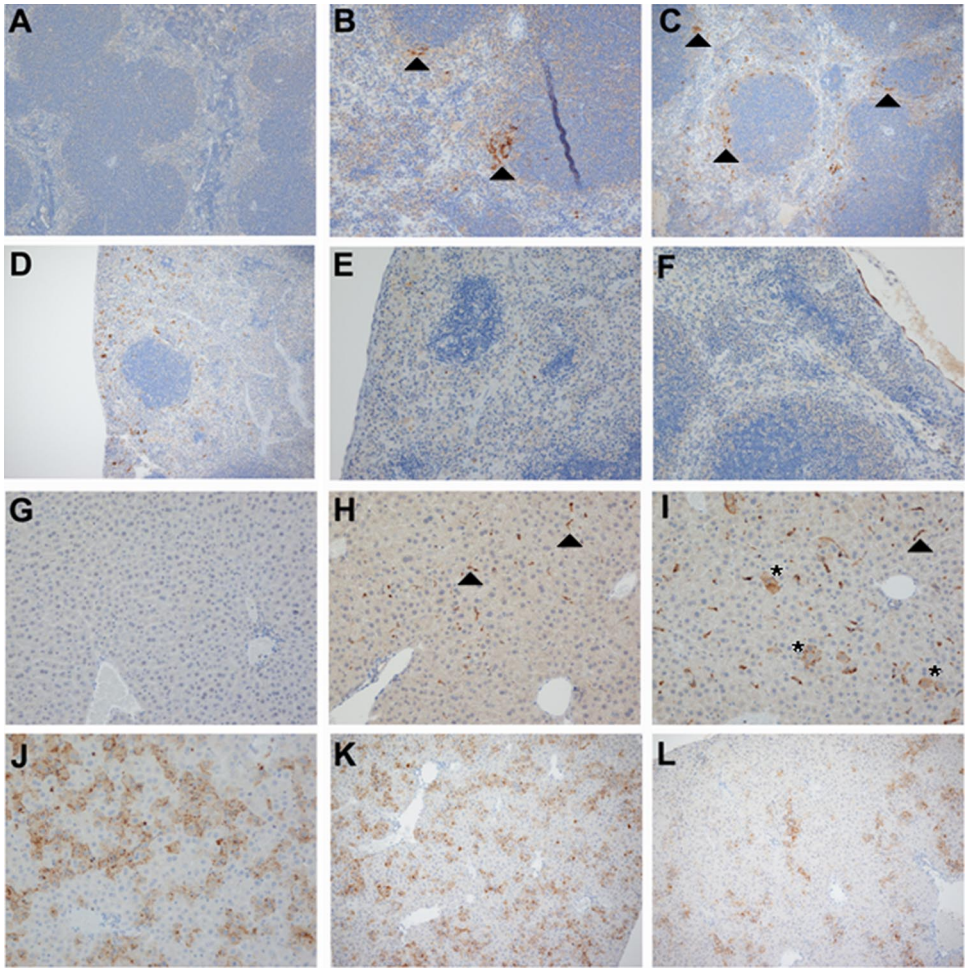

FIG. 4. Immunohistochemical findings in spleens and livers of mice infected with MARV. Immunohistochemical staining was conducted on the spleens and livers of MARV-infected mice, and representative pictures of each tissue from days 0 (A and G), 2 (B and H), 3 (C and I), 4 (D and J), 5 (E and K), and 6 (F and L) are shown. MARV antigen appears brown in both hepatic and splenic sections. (A and G) The spleens and livers of the control (uninfected) mouse sampled at day 0 showed no evidence of MARV antigen. (B and C) In the spleen, the strongest and most consistent MARV antigen staining was observed on day 3 and appeared to be localized to macrophages and dendritic cells in the follicular marginal zones and perilymphoid/perifollicular red pulp (arrowheads). (D to F) Immunohistochemical staining in the spleens of infected mice on days 4, 5, and 6 shows a progressive decrease in both cellular and noncellular MARV antigen. (H) In the livers of MARV-infected mice on day 2, MARV antigen was first localized to small numbers of plump sinusoidal lining cells morphologically consistent with Kupffer cells (arrowheads). (I to K) Hepatocellular staining, noticeable by day 3 and progressively worsening through day 5, was most prominently associated with the cellular membranes of necrotic hepatocytes and with the sinusoids (asterisks). MARV antigen was also localized to areas of inflammation. (L) On day 6, there was decreased hepatic MARV immunostaining, where most viral antigen was seen associated with necrotic hepatocytes and foci of inflammation rather than with pale, swollen, and vacuolated (fatty degeneration) hepatocytes. Magnification, ×10 for panels A to D, K, and L and ×20 for panels E, F, and G to J.

sequence differences to the process of mouse adaptation is unclear at this time. This can be examined in the future through the use of reverse genetic mutations to introduce these changes into the progenitor sequence and subsequently to perform challenge experiments with mice and the mutated viruses. The mutations we identified for mouse adaptation of MARV-Ravn differ from those required for mouse adaptation of EBOV (7, 12). The filovirus VP40 matrix protein is required for viral assembly and budding, and changes in the VP40 protein may increase viral replication or fitness (48). Interestingly, the amino acid mutation identified in VP40 also occurs in guinea pig-adapted MARVs that we have previously described and is located in a nonconserved loop structure between two domains that are homologues only among MARV isolates (31). The NP is tightly associated with the viral RNA, and together with L, VP30, and VP35, it forms the nucleocapsid complex (4). Furthermore, the VP35 protein is an IFN antagonist (2, 3, 9), and IFN responses have been suspected to be responsible for resistance of mice to primary filovirus isolates (6). It was surprising that we did not find changes in VP24, as it is also thought to be an IFN antagonist and important for mouse adaptation of EBOV (12, 13, 28, 39), or GP, which is the attachment protein and immunodominant viral protein. It was also surprising to us that there were no amino acid mutations in the L protein, as it along with VP35 forms the RNA-dependent RNA polymerase (4) and mutations in either of

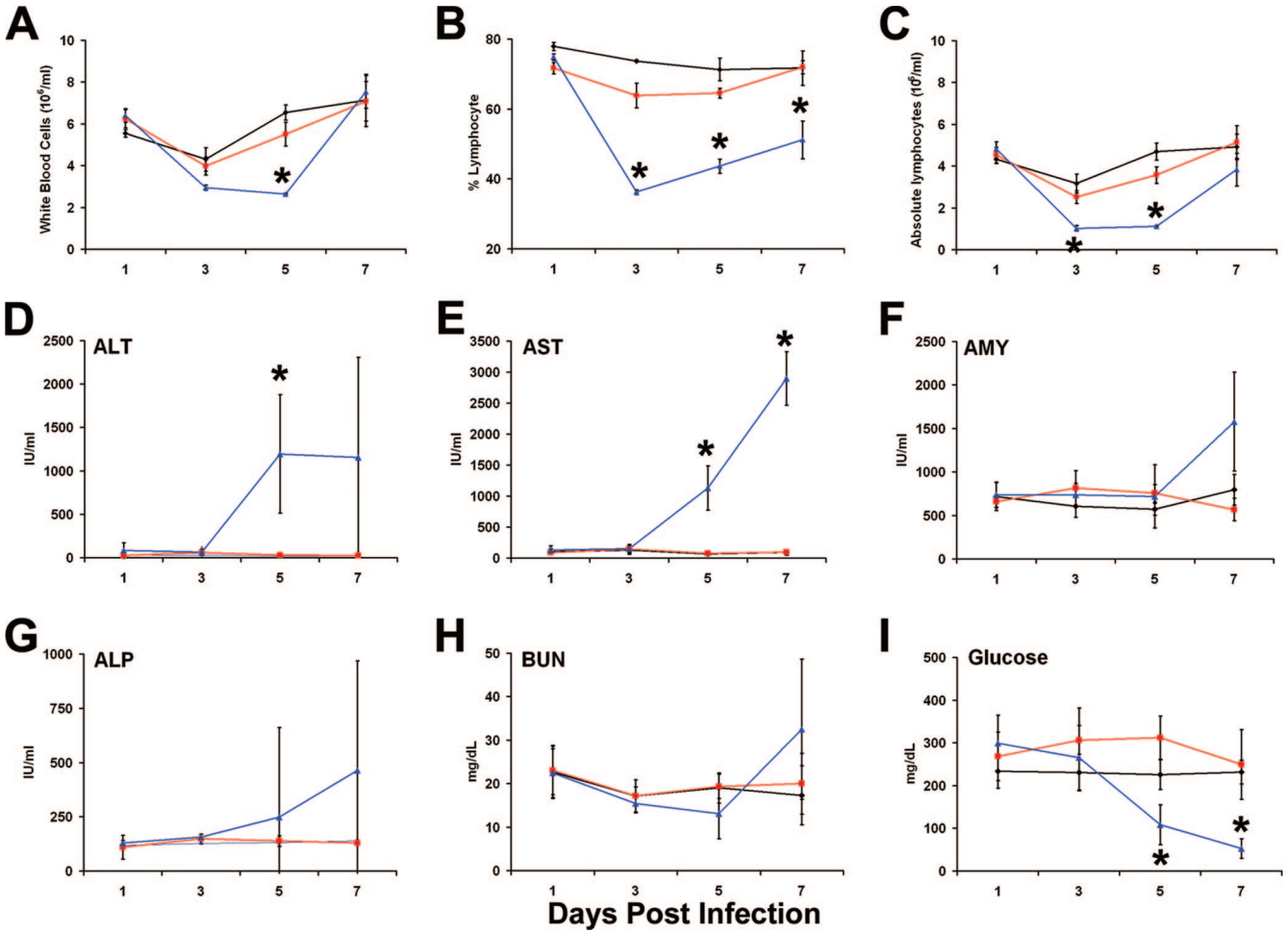

FIG. 5. Serum chemistry and hematology values for BALB/c mice infected with mouse-adapted MARV. Mice were infected with 1,000 PFU of wt or mouse-adapted MARV-Ravn, and whole blood or sera were collected at the indicated times. (A to C) Whole blood was collected from individual mice (n = 4 or 5/time point) in EDTA via terminal cardiac puncture at the indicated time points and was analyzed using a Coulter counter. (A) Total numbers of white blood cells. (B) Percentages of lymphocytes. (C) Absolute numbers of lymphocytes. Data are presented as mean values ± standard deviations. Levels of ALT (D), AST (E), amylase (AMY) (F), ALP (G), BUN (H), and glucose (I) were measured in serum samples from naïve (black lines) or wt (red lines) or mouse-adapted (blue lines) MARV-Ravn-infected mice. Data are expressed as the average of values for five to nine mice/time point, and error bars indicate standard deviations. *, $P \leq 0.05$ (comparing naïve and mouse-adapted MARV-Ravn-infected mice).

these proteins might alter viral replication rates (20, 52). A benefit of nonhuman primate models is their susceptibility to primary human MARV isolates. However, ma-MARV has very few amino acid changes compared to the progenitor (16 of ~6,000 amino acids, or <0.3% mutation from the parental primary isolate), and thus it remains remarkably similar to the progenitor virus derived from a human case of MHF. There is evidence that mouse-adapted EBOV is somewhat attenuated in nonhuman primates (7); whether this is the case for ma-MARV-Ravn awaits further study.

It has been proposed that the pathogenesis of EBOV and MARV infections in nonhuman primates most closely mirrors that seen in human disease, although the pathology data after human disease are scarce (14, 16, 17, 25). Experimental infection of nonhuman primates with MARV results in an incubation period of 2 to 6 days before laboratory and clinical changes begin to occur, with death typically occurring 8 to 11 days after parenteral infection, or longer for mucosal inoculation (24, 32, 34). The clinical signs of MHF in nonhuman primates include fever, anorexia, maculopapular rash, huddling, weight loss, dehydration, diarrhea, prostration, failure to respond to stimulation, hind-limb paralysis, and rarely, bleeding from body orifices. Therefore, many of the clinical observations for the mouse and nonhuman primate MARV infection models are similar. The most notable dissimilarities for mice compared to nonhuman primates are the lack of susceptibility to wt viruses and susceptibility to a single route of infection. Additionally, the 50% lethal dose may be slightly higher for the mouse model than for the nonhuman primate model (<42 PFU based on a single study [data not shown]). However, the incubation period, time to death, and many of the other clinical signs were similar in both the mouse and nonhuman primate models.

Serial sampling studies to characterize the pathogenesis of ma-MARV (Fig. 3 and 4) indicated additional similarities to filovirus disease observed in other models, including guinea

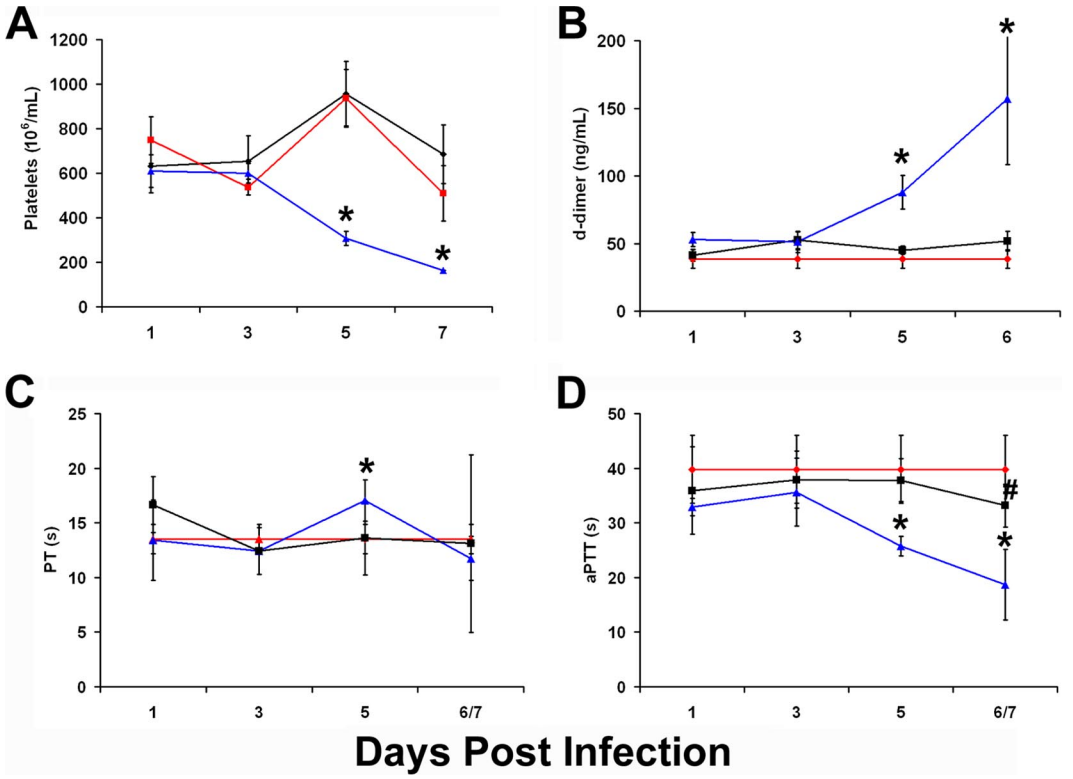

FIG. 6. Changes in coagulation function in MARV-Ravn-infected mice. Mice were infected with 1,000 PFU of wt or mouse-adapted MARV-Ravn, and whole blood or sera were collected at the indicated times. (A) Whole blood was collected from individual mice in EDTA via terminal cardiac puncture at the indicated time points and was analyzed using a Coulter counter for the total number of platelets. (B) D-dimer levels in MARV-infected mice. (C and D) Clotting times (PT and aPTT) were determined using a ThromboScreen. Data in panels A to D for naïve (red lines) or wt (black lines) or mouse-adapted (blue lines) MARV-Ravn-infected mice are expressed as the average of values for four or five mice/time point, and error bars indicate standard deviations. *, $P \leq 0.05$ (comparing naïve and mouse-adapted MARV-Ravn-infected mice); #, $P \leq 0.05$ (comparing naïve and wt-MARV-Ravn-infected mice).

pigs and nonhuman primates (10, 16, 24, 29, 34, 40–43, 45–47, 50, 54). Principle gross necropsy lesions in guinea pigs and nonhuman primates after MARV infection include splenomegaly, enlarged fatty liver, enlarged mesenteric lymph nodes, consolidated hemorrhagic areas in the lungs, and vascular congestion and petechial and/or ecchymotic hemorrhage in the gastrointestinal tract, reproductive organs, adrenal glands, pancreas, liver, spleen, brain, and heart (24, 32, 34, 40, 45, 49, 51, 54). Initial microscopic lesions in MARV-infected guinea pigs and nonhuman primates arise in the mononuclear phagocytic system of the liver and spleen (24, 32, 34, 40, 45, 54). Later notable microscopy observations of MARV-infected guinea pigs and nonhuman primates include multifocal necrosis of liver tissue with the presence of apoptotic bodies and evidence of fatty degeneration, and depletion or complete destruction of the while pulp in the spleen and lymph nodes is observed, along with red pulp disruption due to deposition of cellular debris (17, 30, 34, 35, 44, 45, 54). Lymphocyte apoptosis is a common finding in acute, severe infections (1, 15, 36, 37). In some cases, such as septic shock, inhibition of lymphocyte apoptosis can diminish the pathogenesis of infection (32). Several host factors, including TRAIL, FasL, and nitric oxide, have been proposed to cause lymphocyte apoptosis in filovirus infection (18, 21, 26). It has also been suggested that lymphopenia and destruction of lymphocytes during filovirus infection may be due to a retrovirus-like peptide within the GP (53), although the precise mechanism for this model is not yet established. It is interesting that viremia, as well as MARV antigen staining in the tissues, decreases over time in animals infected with lethal ma-MARV (Fig. 4). This may be due to active and functional immune responses, as observed in the EBOV mouse model (5).

Furthermore, the majority of the changes observed in the blood of mice infected with ma-MARV are very similar to those observed in nonhuman primates. Early hematological changes include profound lymphopenia, variable neutrophilia, and profound thrombocytopenia beginning around day 5 or 6 of the infection. Furthermore, liver function appears to be impaired drastically in MARV-infected mice, similar to effects seen in infected nonhuman primates. Increases in BUN levels were also observed, with only mild elevations (two- to fivefold) in creatinine levels, and this may reflect either kidney damage or effects of hypovolemia. The most obvious difference in the mouse model of MHF compared to the nonhuman primate disease is in coagulopathy. The mice had profound thrombocytopenia, hemorrhage, and uncontrolled bleeding after lethal MARV-Ravn infection and also had elevations in D-dimers (fibrin degradation products), although no significant alterations in clotting times were observed (Fig. 6). It was previously noted for mouse-adapted EBOV that rodents do not

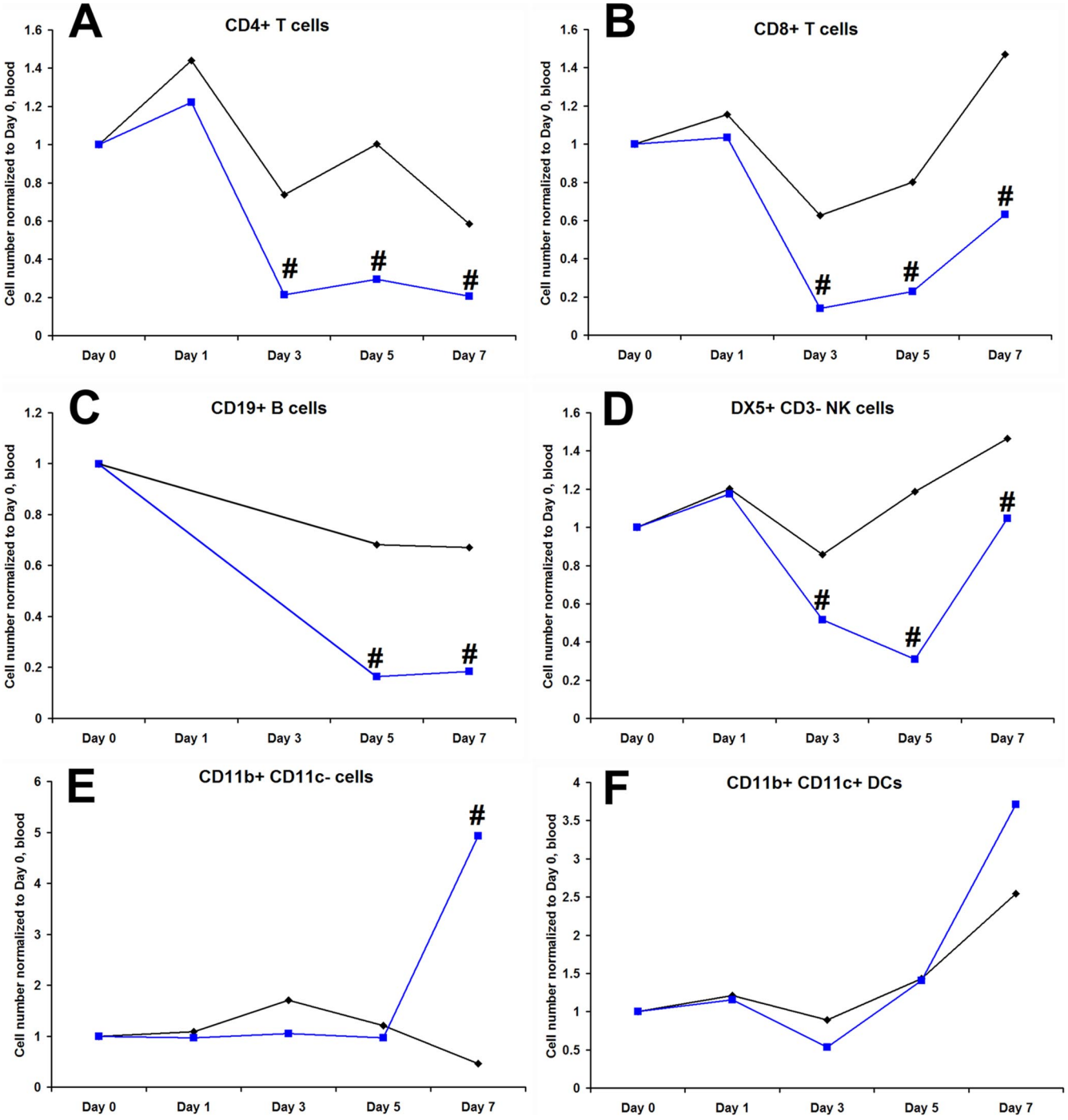

FIG. 7. Cellular immune responses to wt and mouse-adapted MARV-Ravn infection. To determine the cellular changes after MARV-Ravn infection, mice were infected with 1,000 PFU of wt or mouse-adapted MARV-Ravn, whole blood was collected at the indicated time points, and changes in the cell populations, including CD4 and CD8 T cells, B cells ($CD19^+$), NK cells ($DX5^+$ $CD3^-$), monocytes/macrophages ($CD11b^+$ $CD11c^-$), and dendritic cells ($CD11b^+$ CD11c), were analyzed using flow cytometry. Data for wt (black lines) and mouse-adapted (blue lines) MARV-Ravn-infected mice were expressed as changes in cell number normalized to day 0 and were compiled from two separate experiments using five mice/time point/study. #, $P < 0.05$ between wt and mouse-adapted MARV-infected mice.

exhibit the full range of symptoms of disseminated intravascular coagulation that filovirus-infected nonhuman primates often show, including prolongation of PT and aPTT and increased tissue fibrin deposition (8). However, unless the clotting cascade is severely disturbed due to disseminated intravascular coagulation and consumption of clotting factors, there may not be prolongations of the PT or PTT. PT and PTT are only crude measures of coagulation in vivo, and more elaborate studies of clotting factors will be required to differentiate between the observations in mice and nonhuman pri-

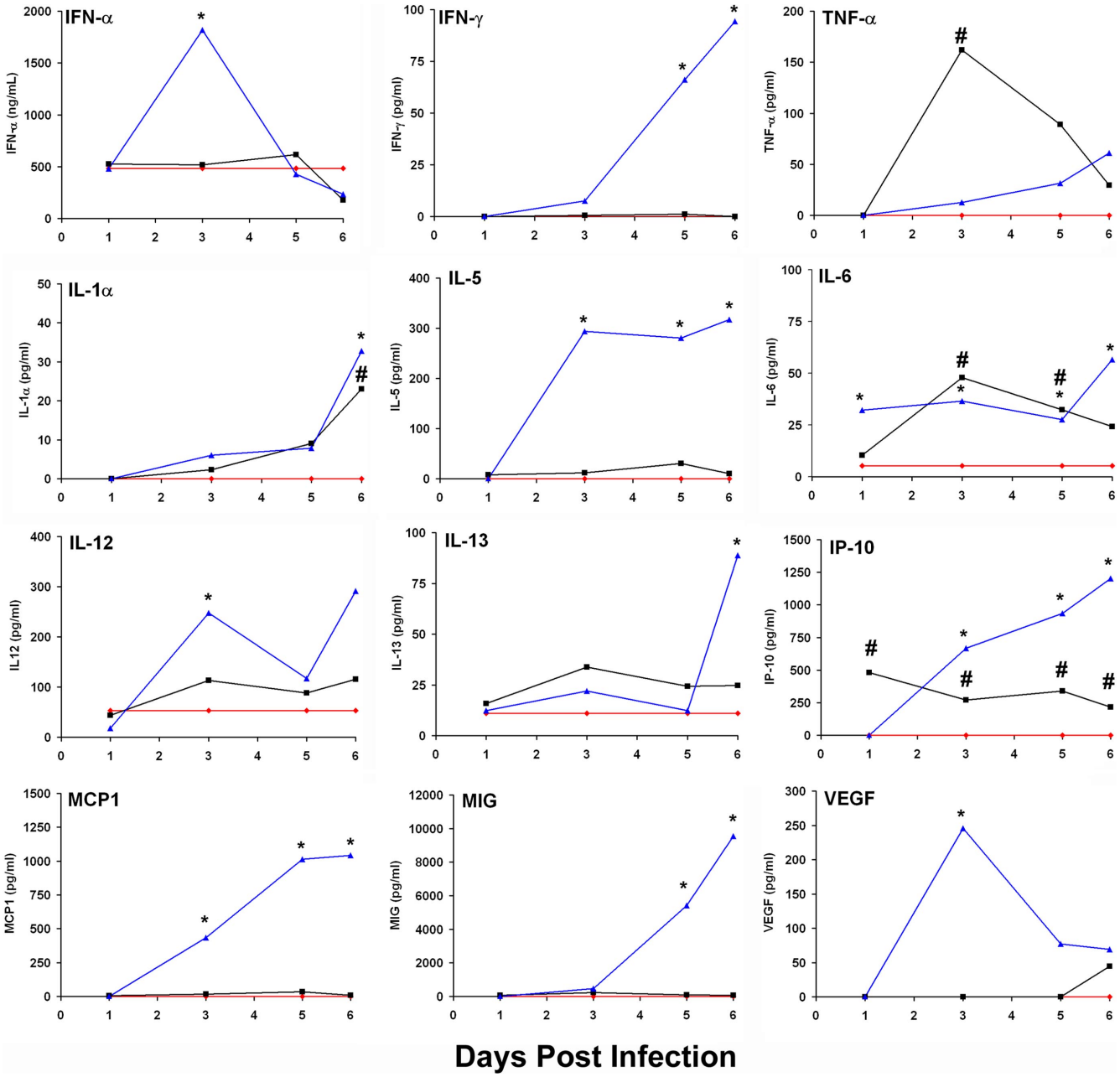

FIG. 8. Cytokine responses to wt and mouse-adapted MARV-Ravn infection. To determine the cytokine changes after MARV-Ravn infection, BALB/c mice were infected with 1,000 PFU of wt or mouse-adapted MARV-Ravn, sera were collected at the indicated time points, and levels of cytokines were measured using a Luminex assay or enzyme-linked immunosorbent assay (IFN-α only). Data for wt (black lines) or mouse-adapted (blue lines) MARV-Ravn-infected mice were expressed as means. Error bars indicate standard errors. *, $P \leq 0.05$ (comparing wt and mouse-adapted MARV-Ravn-infected mice).

mates. Regarding the lack of fibrin tissue deposition in the mouse model, there must be repeated bouts of coagulation sufficient to deplete plasminogen activator in order to see fibrin thrombi. In the presence of plasmin, fibrin thrombi lyse before they can deposit. Therefore, D-dimers may be all that can be seen to reflect the increase in coagulation without clot formation. Nonetheless, it appears that there are differences in mouse physiology that may affect clotting cascades and fibrin deposition.

In our current work, we used a novel approach to adapt a wt isolate of MARV that was avirulent in rodents by first adapting the virus to mice lacking a competent immune system (SCID mice). Once the virus was adapted to SCID mice, the virus was further adapted using BALB/c mice in the context of an intact immune system. This novel method of utilizing genetically altered mice to adapt primary virus isolates may prove broadly applicable to other viruses lacking mouse models. Furthermore, we developed a model which may allow for rapid screen-

TABLE 1. Sequence differences in wt-MARV and ma-MARV[a]

Gene	Nucleotide			Amino acid		
	No.	WT	MA	No.	WT	MA
NP	731	T	C	210	Y	H
	733	T	C			
	739	T	C			
VP35	3044	T	C	34	Y	H
	3072	T	C	43	V	A
	3077	T	C	45	L	P
	3078	T	C			
	3083	T	C	47	C	R
	3085	T	C			
	3129	T	C	62	V	A
IR VP35/VP40	4134	T	C			
	4139	T	C			
	4157	T	C			
	4173	T	C			
	4174	T	C			
	4188	T	C			
	4217	T	C			
VP40	4586	T	C	7	Y	H
	4588	T	C			
	4621	T	C			
	4622	T	C	19	Y	H
	4627	T	C			
	4630	T	C			
	4737	T	C	57	V	A
	4738	T	C			
	5060	A	G	165	T	A
	5117	G	A	184	D	N
	5133	A	G	189	N	S
	5135	A	G	190	T	A
IR GP/VP30	8268	T	C			
	8284	T	C			
	8290	T	C			
	8298	T	C			
	8301	T	C			
	8305	T	C			
	8307	T	C			
	8308	T	C			
	8334	T	C			
	8337	T	C			
	8339	T	C			
	8340	T	C			
	8341	T	C			
	8342	T	C			
	8376	T	C			
	8390	T	C			
	8391	T	C			
	8399	T	C			
	8410	T	C			
	8411	T	C			
	8419	T	C			
	8423	T	C			
	8425	T	C			
	8429	T	C			
	8440	T	C			
	8447	T	C			
	8448	T	C			
	8454	T	C			
	8457	T	C			
	8600	A	G			
VP30	9010	A	G	48	T	A
L	16375	T	C			
Trailer	19068	T	C			

[a] WT, wild-type progenitor virus derived from a human infected with MARV-Ravn; MA, mouse-adapted virus that is lethal in BALB/c mice.

ing of novel MARV-specific therapeutics and prophylactics as well as for dissection of the pathogenesis and immunology of MARV infection.

ACKNOWLEDGMENTS

We thank C. Rice, I. Alexander, and D. Braun for excellent technical assistance, K. Kenyon for reviewing the manuscript, and W. V. Kalina, D. L. Swenson, J. G. Perkins, G. G. Olinger, J. Dye, L. E. Hensley, M. J. Aman, A. O. Anderson, and A. L. Schmaljohn for insightful discussions.

A portion of the research described herein was sponsored by the Defense Threat Reduction Agency JSTO-CBD and the Medical Research and Materiel Command.

Opinions, interpretations, conclusions, and recommendations are those of the authors and are not necessarily endorsed by the U.S. Army.

REFERENCES

1. **Ahmeti, S., and L. Raka.** 2006. Crimean-Congo haemorrhagic fever in Kosova: a fatal case report. Virol. J. **3:**85.
2. **Basler, C. F., A. Mikulasova, L. Martinez-Sobrido, J. Paragas, E. Muhlberger, M. Bray, H. D. Klenk, P. Palese, and A. Garcia-Sastre.** 2003. The Ebola virus VP35 protein inhibits activation of interferon regulatory factor 3. J. Virol. **77:**7945–7956.
3. **Basler, C. F., X. Wang, E. Muhlberger, V. Volchkov, J. Paragas, H. D. Klenk, A. Garcia-Sastre, and P. Palese.** 2000. The Ebola virus VP35 protein functions as a type I IFN antagonist. Proc. Natl. Acad. Sci. USA **97:**12289–12294.
4. **Becker, S., C. Rinne, U. Hofsass, H. D. Klenk, and E. Muhlberger.** 1998. Interactions of Marburg virus nucleocapsid proteins. Virology **249:**406–417.
5. **Bradfute, S. B., K. L. Warfield, and S. Bavari.** 2008. Functional CD8+ T cell responses in lethal Ebola virus infection. J. Immunol. **180:**4058–4066.
6. **Bray, M.** 2001. The role of the type I interferon response in the resistance of mice to filovirus infection. J. Gen. Virol. **82:**1365–1373.
7. **Bray, M., K. Davis, T. Geisbert, C. Schmaljohn, and J. Huggins.** 1998. A mouse model for evaluation of prophylaxis and therapy of Ebola hemorrhagic fever. J. Infect. Dis. **178:**651–661.
8. **Bray, M., S. Hatfill, L. Hensley, and J. W. Huggins.** 2001. Haematological, biochemical and coagulation changes in mice, guinea-pigs and monkeys infected with a mouse-adapted variant of Ebola Zaire virus. J. Comp. Pathol. **125:**243–253.
9. **Cardenas, W. B., Y. M. Loo, M. Gale, Jr., A. L. Hartman, C. R. Kimberlin, L. Martinez-Sobrido, E. O. Saphire, and C. F. Basler.** 2006. Ebola virus VP35 protein binds double-stranded RNA and inhibits alpha/beta interferon production induced by RIG-I signaling. J. Virol. **80:**5168–5178.
10. **Connolly, B. M., K. E. Steele, K. J. Davis, T. W. Geisbert, W. M. Kell, N. K. Jaax, and P. B. Jahrling.** 1999. Pathogenesis of experimental Ebola virus infection in guinea pigs. J. Infect. Dis. **179**(Suppl. 1)**:**S203–S217.
11. **Daddario-DiCaprio, K. M., T. W. Geisbert, J. B. Geisbert, U. Stroher, L. E. Hensley, A. Grolla, E. A. Fritz, F. Feldmann, H. Feldmann, and S. M. Jones.** 2006. Cross-protection against Marburg virus strains by using a live, attenuated recombinant vaccine. J. Virol. **80:**9659–9666.
12. **Ebihara, H., A. Takada, D. Kobasa, S. Jones, G. Neumann, S. Theriault, M. Bray, H. Feldmann, and Y. Kawaoka.** 2006. Molecular determinants of Ebola virus virulence in mice. PLoS Pathog. **2:**e73.
13. **Feng, Z., M. Cerveny, Z. Yan, and B. He.** 2007. The VP35 protein of Ebola virus inhibits the antiviral effect mediated by double-stranded RNA-dependent protein kinase PKR. J. Virol. **81:**182–192.
14. **Fisher-Hoch, S. P., G. S. Platt, G. Lloyd, D. I. Simpson, G. H. Neild, and A. J. Barrett.** 1983. Haematological and biochemical monitoring of Ebola infection in rhesus monkeys: implications for patient management. Lancet **ii:** 1055–1058.
15. **Flick, R., and M. Bouloy.** 2005. Rift Valley fever virus. Curr. Mol. Med. **5:**827–834.
16. **Gedigk, P., H. Bechtelsheimer, and G. Korb.** 1968. Pathological anatomy of the "Marburg virus" disease (the so-called "Marburg monkey disease"). Dtsch. Med. Wochenschr. **93:**590–601.
17. **Geisbert, T., P. Jahrling, T. Larsen, K. Davis, and L. E. Hensley.** 2004. Filovirus pathogenesis in nonhuman primates, p. 203–238. *In* H. Klenk and H. Feldmann (ed.), Ebola and Marburg viruses: molecular and cellular biology. Horizon Bioscience, Norfolk, United Kingdom.
18. **Geisbert, T. W., L. E. Hensley, T. R. Gibb, K. E. Steele, N. K. Jaax, and P. B. Jahrling.** 2000. Apoptosis induced in vitro and in vivo during infection by Ebola and Marburg viruses. Lab Investig. **80:**171–186.
19. **Geisbert, T. W., L. E. Hensley, P. B. Jahrling, T. Larsen, J. B. Geisbert, J. Paragas, H. A. Young, T. M. Fredeking, W. E. Rote, and G. P. Vlasuk.** 2003. Treatment of Ebola virus infection with a recombinant inhibitor of factor VIIa/tissue factor: a study in rhesus monkeys. Lancet **362:**1953–1958.
20. **Geisbert, T. W., L. E. Hensley, E. Kagan, E. Z. Yu, J. B. Geisbert, K.**

Daddario-DiCaprio, E. A. Fritz, P. B. Jahrling, K. McClintock, J. R. Phelps, A. C. Lee, A. Judge, L. B. Jeffs, and I. MacLachlan. 2006. Postexposure protection of guinea pigs against a lethal Ebola virus challenge is conferred by RNA interference. J. Infect. Dis. **193:**1650–1657.

21. **Geisbert, T. W., L. E. Hensley, T. Larsen, H. A. Young, D. S. Reed, J. B. Geisbert, D. P. Scott, E. Kagan, P. B. Jahrling, and K. J. Davis.** 2003. Pathogenesis of Ebola hemorrhagic fever in cynomolgus macaques: evidence that dendritic cells are early and sustained targets of infection. Am. J. Pathol. **163:**2347–2370.
22. **Gibb, T. R., M. Bray, T. W. Geisbert, K. E. Steele, W. M. Kell, K. J. Davis, and N. K. Jaax.** 2001. Pathogenesis of experimental Ebola Zaire virus infection in BALB/c mice. J. Comp. Pathol. **125:**233–242.
23. **Gonchar, N. I., V. A. Pshenichnov, V. A. Pokhodiaev, K. L. Lopatov, and I. V. Firsova.** 1991. The sensitivity of different experimental animals to the Marburg virus. Vopr. Virusol. **36:**435–437.
24. **Haas, R., and G. Maass.** 1971. Experimental infection of monkeys with the Marburg virus, p. 136–143. *In* G. A. Martini and R. Siegert (ed.), Marburg virus. Springer-Verlag, New York, NY.
25. **Hart, M. K.** 2003. Vaccine research efforts for filoviruses. Int. J. Parasitol. **33:**583–595.
26. **Hensley, L. E., H. A. Young, P. B. Jahrling, and T. W. Geisbert.** 2002. Proinflammatory response during Ebola virus infection of primate models: possible involvement of the tumor necrosis factor receptor superfamily. Immunol. Lett. **80:**169–179.
27. **Hoenen, T., A. Groseth, D. Falzarano, and H. Feldmann.** 2006. Ebola virus: unravelling pathogenesis to combat a deadly disease. Trends Mol. Med. **12:**206–215.
28. **Hoenen, T., A. Groseth, L. Kolesnikova, S. Theriault, H. Ebihara, B. Hartlieb, S. Bamberg, H. Feldmann, U. Stroher, and S. Becker.** 2006. Infection of naive target cells with virus-like particles: implications for the function of Ebola virus VP24. J. Virol. **80:**7260–7264.
29. **Ignatev, G. M., A. P. Agafonov, M. A. Strel'tsova, V. A. Kuz'min, G. I. Mainagasheva, G. V. Spirin, and N. B. Chernyi.** 1991. A comparative study of the immunological indices in guinea pigs administered an inactivated Marburg virus. Vopr. Virusol. **36:**421–423.
30. **Jaax, N. K., K. J. Davis, T. J. Geisbert, P. Vogel, G. P. Jaax, M. Topper, and P. B. Jahrling.** 1996. Lethal experimental infection of rhesus monkeys with Ebola-Zaire (Mayinga) virus by the oral and conjunctival route of exposure. Arch. Pathol. Lab. Med. **120:**140–155.
31. **Lofts, L. L., M. S. Ibrahim, D. L. Negley, M. C. Hevey, and A. L. Schmaljohn.** 2007. Genomic differences between guinea pig lethal and nonlethal Marburg virus variants. J. Infect. Dis. **196**(Suppl. 2)**:**S305–S312.
32. **Lub, M. Y., A. N. Sergeev, O. V. P'yankov, O. G. P'yankova, V. A. Petrishchenko, and L. A. Kotlyarov.** 1995. Certain pathogenetic characteristics of a disease in monkeys aerogenically infected with the Marburg virus. Vopr. Virusol. **40:**158–161.
33. **Moe, J. B., R. D. Lambert, and H. W. Lupton.** 1981. Plaque assay for Ebola virus. J. Clin. Microbiol. **13:**791–793.
34. **Murphy, F. A., D. I. Simpson, S. G. Whitfield, I. Zlotnik, and G. B. Carter.** 1971. Marburg virus infection in monkeys. Ultrastructural studies. Lab. Investig. **24:**279–291.

34a. **National Research Council.** 1996. Guide for the care and use of laboratory animals. National Academy Press, Washington, DC.

35. **Oehlert, W.** 1971. The morphologic picture in livers, spleens, and lymph nodes of monkeys and guinea pigs after infections with the "vervet agent," p. 144–156. *In* G. A. Martini and R. Siegert (ed.), Marburg virus. Springer-Verlag, New York, NY.
36. **Parrino, J., R. S. Hotchkiss, and M. Bray.** 2007. Prevention of immune cell apoptosis as potential therapeutic strategy for severe infections. Emerg. Infect. Dis. **13:**191–198.
37. **Peiris, J. S., K. Y. Yuen, A. D. Osterhaus, and K. Stohr.** 2003. The severe acute respiratory syndrome. N. Engl. J. Med. **349:**2431–2441.
38. **Reed, D. S., L. E. Hensley, J. B. Geisbert, P. B. Jahrling, and T. W. Geisbert.** 2004. Depletion of peripheral blood T lymphocytes and NK cells during the course of Ebola hemorrhagic fever in cynomolgus macaques. Viral Immunol. **17:**390–400.
39. **Reid, S. P., L. W. Leung, A. L. Hartman, O. Martinez, M. L. Shaw, C. Carbonnelle, V. E. Volchkov, S. T. Nichol, and C. F. Basler.** 2006. Ebola virus VP24 binds karyopherin alpha1 and blocks STAT1 nuclear accumulation. J. Virol. **80:**5156–5167.
40. **Robin, Y., P. Bres, and R. Camain.** 1971. Passage of Marburg virus in guinea pigs, p. 117–122. *In* G. A. Martini and R. Siegert (ed.), Marburg virus. Springer-Verlag, New York, NY.
41. **Ryabchikova, E., L. Kolesnikova, M. Smolina, V. Tkachev, L. Pereboeva, S. Baranova, A. Grazhdantseva, and Y. Rassadkin.** 1996. Ebola virus infection in guinea pigs: presumable role of granulomatous inflammation in pathogenesis. Arch. Virol. **141:**909–921.
42. **Ryabchikova, E., L. Strelets, L. Kolesnikova, O. P'yankov, and A. Sergeev.** 1996. Respiratory Marburg virus infection in guinea pigs. Arch. Virol. **141:** 2177–2190.
43. **Shu, H. L., R. Siegert, and W. Slenczka.** 1969. The pathogenesis and epidemiology of the "Marburg-virus" infection. Ger. Med. Mon. **14:**7–10.
44. **Simpson, D. I.** 1969. Marburg agent disease. Trans. R. Soc. Trop. Med. Hyg. **63:**303–309.
45. **Simpson, D. I., I. Zlotnik, and D. A. Rutter.** 1968. Vervet monkey disease: experimental infection of guinea pigs and monkeys with the causative agents. Br. J. Exp. Pathol. **49:**458–464.
46. **Slenczka, W., H. L. Shu, G. Piepenberg, and R. Siegert.** 1968. Detection of the antigen of the "Marburg virus" in the organs of infected guinea-pigs by immunofluorescence. Ger. Med. Mon. **13:**524–529.
47. **Stille, W., and E. Bohle.** 1971. Clinical course and prognosis of Marburg virus ("green-monkey") disease, p. 10–18. *In* G. A. Martini and R. Siegart (ed.), Marburg virus disease. Springer-Verlag, New York, NY.
48. **Swenson, D. L., K. L. Warfield, K. Kuehl, T. Larsen, M. C. Hevey, A. Schmaljohn, S. Bavari, and M. J. Aman.** 2004. Generation of Marburg virus-like particles by co-expression of glycoprotein and matrix protein. FEMS Immunol. Med. Microbiol. **40:**27–31.
49. **Swenson, D. L., K. L. Warfield, T. Larsen, D. A. Alves, S. S. Coberley, and S. Bavari.** 2008. Monovalent virus-like particle vaccine protects guinea pigs and nonhuman primates against infection with multiple Marburg viruses. Expert Rev. Vaccines **7:**417–429.
50. **Volchkov, V. E., A. A. Chepurnov, V. A. Volchkova, V. A. Ternovoj, and H. D. Klenk.** 2000. Molecular characterization of guinea pig-adapted variants of Ebola virus. Virology **277:**147–155.
51. **Warfield, K. L., D. A. Alves, S. B. Bradfute, D. K. Reed, S. Vantongeren, W. V. Kalina, G. G. Olinger, and S. Bavari.** 2007. Development of a model for marburgvirus based on severe-combined immunodeficiency mice. Virol. J. **4:**108.
52. **Warfield, K. L., D. L. Swenson, G. G. Olinger, D. K. Nichols, W. D. Pratt, R. Blouch, D. A. Stein, M. J. Aman, P. L. Iversen, and S. Bavari.** 2006. Gene-specific countermeasures against Ebola virus based on antisense phosphorodiamidate morpholino oligomers. PLoS Pathog. **2:**e1.
53. **Yaddanapudi, K., G. Palacios, J. S. Towner, I. Chen, C. A. Sariol, S. T. Nichol, and W. I. Lipkin.** 2006. Implication of a retrovirus-like glycoprotein peptide in the immunopathogenesis of Ebola and Marburg viruses. FASEB J. **20:**2519–2530.
54. **Zlotnik, I.** 1969. Marburg agent disease: pathology. Trans. R. Soc. Trop. Med. Hyg. **63:**310–323.